J|A|C|S
ARTICLES
Published on Web 03/20/2007

Insertion of Molecular Oxygen into a Palladium−Hydride Bond: Computational Evidence for Two Nearly Isoenergetic Pathways

Brian V. Popp* and Shannon S. Stahl*

Contribution from the Department of Chemistry, University of Wisconsin−Madison, 1101 University Avenue, Madison, Wisconsin 53706

Received December 18, 2006; E-mail: bpopp@chem.wisc.edu; stahl@chem.wisc.edu

Abstract: The reaction of a palladium^{II}−hydride species with molecular oxygen to form palladium^{II}−hydroperoxide has been proposed as a key step in Pd-catalyzed aerobic oxidation reactions. We recently reported one of the first experimental precedents for such a step (*Angew. Chem., Int. Ed.* **2006**, *45*, 2904−2907). DFT calculations have been used to probe the mechanism for this reaction, which consists of formal insertion of O_2 into the palladium−hydride bond of *trans*-$(NHC)_2Pd(H)OAc$ (NHC = *N*-heterocyclic carbene). Four different pathways were considered: (1) hydrogen atom abstraction (HAA) of the Pd−H bond by molecular oxygen, (2) reductive elimination of HX followed by oxygenation of Pd^0 and protonolysis of the (η^2-peroxo)−Pd^{II} species, (3) oxygenation of palladium^{II}−hydride with subsequent reductive elimination of the O−H bond from an η^2-peroxo−Pd^{IV} center, and (4) formation of a *cis*-superoxide adduct of the palladium−hydride species followed by O−H bond formation via hydrogen atom migration. The calculations reveal that pathways 1 and 2 are preferred energetically, and both pathways exhibit very similar kinetic barriers. This result suggests that more than one pathway is possible for catalyst reoxidation in Pd-catalyzed aerobic oxidation reactions.

Introduction

Over the past decade, the scope and utility of palladium-catalyzed aerobic oxidation reactions have expanded significantly.[1] These reactions have been the subject of considerable mechanistic investigation and are generally proposed to proceed through a Pd^{II}/Pd^0 redox cycle analogous to that of well-known Pd-catalyzed cross-coupling reactions (Scheme 1). Several observations lend support to this mechanistic proposal: (1) Pd^{II} is an effective stoichiometric oxidant for a variety of organic substrates ($SubH_2$), (2) Pd^0 is readily oxidized to Pd^{II} in the presence of molecular oxygen and 2 equiv of a Brønsted acid,[2] and (3) the Pd catalyst commonly decomposes into metallic Pd (Pd black) during the reaction, a result that implicates the presence of a Pd^0 intermediate in the catalytic cycle.[3] In spite of this evidence, the oxidation of Pd^0 by molecular oxygen has not been observed directly under catalytic conditions (e.g., via spectroscopy),[3,4] and a number of uncertainties associated with the catalyst reoxidation process remain.

Scheme 1. Traditional Mechanisms for Palladium-Catalyzed Aerobic Oxidation (A) and Cross-Coupling (B) Reactions

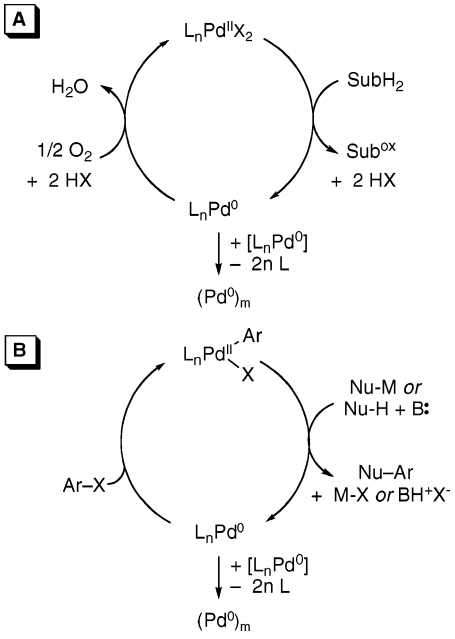

Pd^{II}-mediated oxidations of organic molecules often feature β-hydride elimination as the final step of substrate oxidation, resulting in the formation of a palladium^{II}−hydride intermediate in the catalytic cycle (Scheme 2, intermediate **B**). According to the traditional Pd^{II}/Pd^0 cycle for Pd-catalyzed oxidation reactions, the palladium-hydride intermediate undergoes reductive

(1) (a) Stahl, S. S. *Angew. Chem., Int. Ed.* **2004**, *43*, 3400−3420. (b) Stahl, S. S. *Science* **2005**, *309*, 1824−1826. (c) Sigman, M. S.; Schultz, M. J. *Org. Biomol. Chem.* **2004**, *2*, 2551−2554. (d) Sigman, M. S.; Jensen, D. R. *Acc. Chem. Res.* **2006**, *39*, 221−229. (e) Gligorich, K. M.; Sigman, M. S. *Angew. Chem., Int. Ed.* **2006**, *45*, 6612−6615. (f) Stoltz, B. M. *Chem. Lett.* **2004**, *33*, 362−367. (g) Nishimura, T.; Uemura, S. *Synlett* **2004**, 201−216. (h) Sheldon, R. A.; Arends, I. W. C. E.; ten Brink, G.-J.; Dijksman, A. *Acc. Chem. Res.* **2002**, *35*, 774−781. (i) Toyota, M.; Ihara, M. *Synlett* **2002**, 1211−1222.

(2) (a) Stahl, S. S.; Thorman, J. L.; Nelson, R. C.; Kozee, M. A. *J. Am. Chem. Soc.* **2001**, *123*, 7188−7189. (b) Konnick, M. M.; Guzei, I. A.; Stahl, S. S. *J. Am. Chem. Soc.* **2004**, *126*, 10212−10213.

(3) For extensive discussion of Pd decomposition during catalytic turnover, see: Steinhoff, B. A.; Stahl, S. S. *J. Am. Chem. Soc.* **2006**, *128*, 4348−4355.

10.1021/ja069037v CCC: $37.00

Scheme 2. Catalytic Cycle for Palladium-Catalyzed Aerobic Oxidation Reactions Highlighting Alternate Pathways for Catalyst Reoxidation by Molecular Oxygen

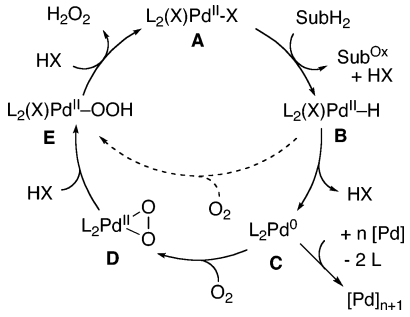

Scheme 3. Migratory Insertion Pathway Proposed for Oxygenation of a Hydrido Palladacyle

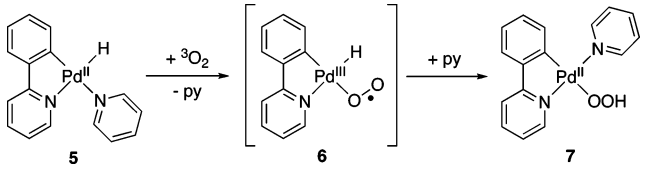

elimination of HX to produce a Pd^0 species (**B** → **C**).[5] Subsequent aerobic oxidation of Pd^0, following the sequence **C** → **D** → **E** → **A** outlined in Scheme 2, has substantial support from experimental studies of well-defined Pd complexes.[2,6]

An alternative catalyst reoxidation mechanism has been proposed that involves direct oxygenation of the palladium^{II}–hydride species **B** to yield the palladium^{II}–hydroperoxide intermediate **E** (Scheme 2, dashed arrow).[7] Until recently, however, no precedent existed for O_2 insertion into a Pd–H bond. The first support for this pathway was provided by computational studies.[8] Moberg et al. investigated the mechanism of aerobic alcohol oxidation with a cyclometallated Pd catalyst using density functional theory (DFT) methods.[8a] They proposed that a palladium^{II}–hydride intermediate (**5**, Scheme 3) reacts with O_2 to form the *cis*-Pd(H)(η^1-O_2) intermediate **6**, which subsequently reacts intramolecularly to form the hydroperoxide species **7**. Stationary points were identified and optimized for each of the ground-state structures shown in Scheme 3, but no transition-state structures or energies were evaluated. The first thorough computational analysis of a palladium–hydride oxygenation pathway was reported by

Scheme 4. HAA Pathway for Oxygenation of [(−)-Sparteine]Pd^{II}(H)Cl

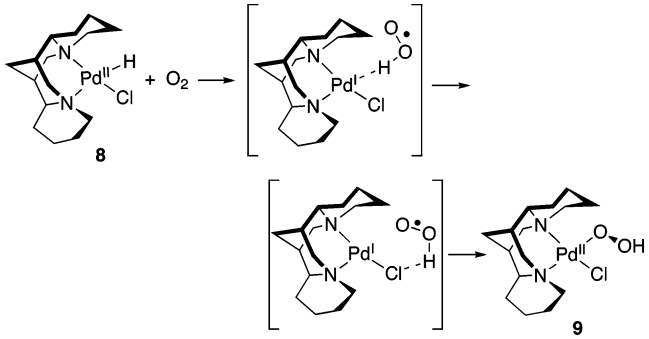

Goddard and co-workers, who evaluated the reaction of molecular oxygen with [(−)-sparteine]Pd^{II}(H)Cl, **8**.[8b] This study revealed that dioxygen insertion into the Pd–H bond of **8** to form the Pd–OOH species **9** should be possible. The low-energy pathway identified in this study consists of a hydrogen atom abstraction (HAA) mechanism (Scheme 4). Namely, molecular oxygen abstracts a hydrogen atom from the Pd center to form a protonated superoxide species, HOO, that interacts weakly with the Pd^I center. Rearrangement of the HOO fragment, mediated by hydrogen bonding to the chloride ligand, enables formation of the Pd–O bond to yield the hydroperoxo–Pd^{II} product.

The first experimental systems were identified shortly after these computational studies. Goldberg et al. reported that molecular oxygen reacts with the palladium–hydride complex ($^{t\mathrm{Bu}}$PCP)PdH, **10** ($^{t\mathrm{Bu}}$PCP = 2,6-bis-[(di-*tert*-butylphosphanyl)-methyl]phenyl), to produce the hydroperoxide species ($^{t\mathrm{Bu}}$PCP)-PdOOH, **11** (eq 1).[9] Independently, our lab observed that molecular oxygen reacts with the *N*-heterocyclic carbene ligated palladium–hydride complex *trans*-$(IMes)_2Pd(H)(O_2CPh)$ (**12**) to afford the corresponding hydroperoxide product **13** (eq 2).[10]

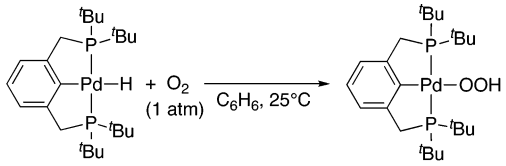

(1)

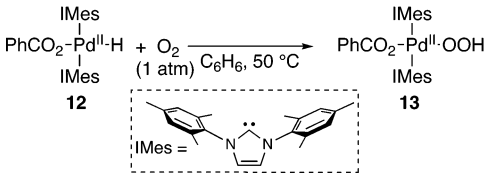

(2)

These well-defined reactions provide an excellent opportunity to probe the mechanism of dioxygen insertion into a palladium–hydride bond and assess the viability of this reaction under catalytic conditions. Kinetic studies of the oxygenation of **10** reveal that the reaction exhibits a bimolecular rate law, first-order in both [Pd–H] and [O_2], and a large deuterium kinetic isotope effect, $k_H/k_D = 5.8$ (Pd–H vs Pd–D).[9] These observa-

(4) The kinetics of catalyst reoxidation tends to be much faster than steps associated with Pd^{II}-mediated substrate oxidation. For leading references to mechanistic studies of reactions under catalytic conditions, see: (a) Mueller, J. A.; Goller, C. P.; Sigman, M. S. *J. Am. Chem. Soc.* **2004**, *126*, 9724–9734. (b) Steinhoff, B. A.; Guzei, I. A.; Stahl, S. S. *J. Am. Chem. Soc.* **2004**, *126*, 11268–11278.

(5) Heck reactions also feature Pd^{II}–hydride species in the catalytic cycle, and a stoichiometric Brønsted base is employed to react with the acid formed upon HX reductive elimination from the Pd–hydride species. For experimental studies of this proposed reactivity, see: (a) Amatore, C.; Jutand, A.; Meyer, G.; Carelli, I.; Chiarotto, I. *Eur. J. Inorg. Chem.* **2000**, 1855–1859. (b) Hills, I. D.; Fu, G. C. *J. Am. Chem. Soc.* **2004**, *126*, 13178–13179.

(6) For computational studies, see: (a) Landis, C. R.; Morales, C. M.; Stahl, S. S. *J. Am. Chem. Soc.* **2004**, *126*, 16302–16303. (b) Zierkiewicz, W.; Privalov, T. *Organometallics* **2005**, *24*, 6019–6028. (c) Nielsen, R. J.; Goddard, W. A., III. *J. Am. Chem. Soc.* **2006**, *128*, 9651–9660. (d) Popp, B. V.; Wendlandt, J. E.; Landis, C. R.; Stahl, S. S. *Angew. Chem., Int. Ed.* **2007**, *46*, 601–604.

(7) For examples, see: (a) Hosokawa, T.; Murahashi, S.-I. *Acc. Chem. Res.* **1990**, *23*, 49–54. (b) Nishimura, T.; Onoue, T.; Ohe, K.; Uemura, S. *J. Org. Chem.* **1999**, *64*, 6750–6755. (c) Muzart, J.; Pete, J. P. *J. Mol. Catal.* **1982**, *15*, 373–376.

(8) (a) Privalov, T.; Linde, C.; Zetterberg, K.; Moberg, C. *Organometallics* **2005**, *24*, 885–893. (b) Keith, J. M.; Nielsen, R. J.; Oxgaard, J.; Goddard, W. A., III. *J. Am. Chem. Soc.* **2005**, *127*, 13172–13179.

(9) Denney, M. C.; Smythe, N. A.; Cetto, K. L.; Kemp, R. A.; Goldberg, K. I. *J. Am. Chem. Soc.* **2006**, *128*, 2508–2509.

(10) Konnick, M. M.; Gandhi, B. A.; Guzei, I. A.; Stahl, S. S. *Angew. Chem., Int. Ed.* **2006**, *45*, 2904–2907.

Scheme 5. Mechanistic Pathways for Reaction of O_2 with Palladium^{II}−Hydride to Produce a Palladium^{II}−Hydroperoxide[a]

1. Hydrogen-Atom-Abstraction Pathway

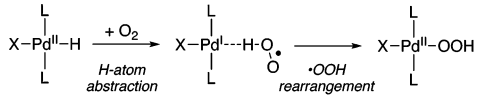

2. HX Reductive Elimination Pathway

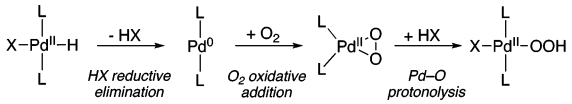

3. Peroxo-Pd^{IV} Pathway

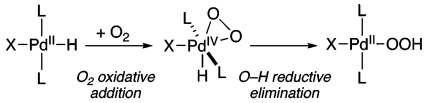

4. O_2 Insertion Pathway

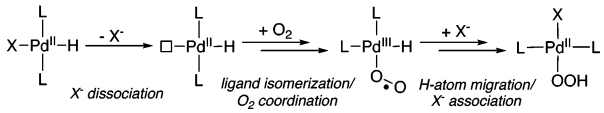

[a] L = IMe and X = OAc.

tions together with results of a recent computational study[11] support an HAA mechanism analogous to that shown in Scheme 4.

The reaction of **12** with O_2 is less well-understood mechanistically. In the initial studies, it was observed that the rate increased significantly when the reaction was performed in the presence of catalytic quantities of carboxylic acid. The mechanistic origin of this effect is not obvious; however, it suggests that the reaction of molecular oxygen with **12** might proceed by a different mechanism than with **10**.[12] To gain insight into these issues, we have been investigating the oxygenation of palladium−hydride complexes analogous to **12** both experimentally and computationally. Here, we present the outcome of a DFT analysis of the reaction between *trans*-(IMe)$_2$Pd(H)-OAc (**14**) and O_2, in which several different mechanisms were considered (Scheme 5): (1) an HAA pathway analogous to that in Scheme 4, (2) a three-step sequence consisting of reductive elimination of HX, oxidative addition of O_2 to Pd^0, and protonolysis of a Pd−O bond of an (η^2-peroxo)−Pd^{II} species, (3) oxidative addition of O_2 to the Pd^{II} center followed by reductive elimination of an O−H bond from an η^2-peroxo−Pd^{IV} center, and (4) formal insertion of O_2 into a Pd^{II}−H bond via hydrogen atom migration to a coordinated superoxide. The calculations reveal that mechanisms 1 and 2 are energetically preferred and that they possess very similar kinetic barriers. The reductive elimination sequence (pathway 2), however, best explains the observations made in our initial experimental studies. We also find that the barrier for the HAA mechanism (pathway 1) is strongly dependent on the identity of the ligand trans to the hydride. Strong donor ligands, as in **10**, significantly lower the barrier for the HAA mechanism (pathway 1). Overall, this study suggests that more than one mechanism is possible for catalyst reoxidation in palladium-catalyzed aerobic oxidation reactions and that the operative mechanism will depend on the identity of the catalyst and the reaction conditions.

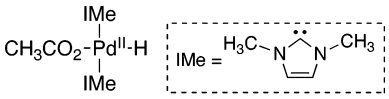

14

Computational Methods

All computations were performed within the Gaussian 03 (G03) electronic structure suite of programs, unless otherwise specified.[13] Spin-unrestricted density functional theory (UDFT)[14] with the hybrid density functional, B3LYP,[15,16] was used for all calculations. A triple-ζ basis set and effective core potential, Stuttgart RSC 1997 ECP,[17] were used on Pd, and the all-electron 6-31+G(d) basis set (Basis A)[18] was used for all other atoms in geometry optimizations and normal-mode analyses. At the calculated stationary points, solvation-corrected single-point energy calculations were carried out with the Pd basis detailed previously and the 6-311++G(d,p) basis on all other atoms (Basis B) with electrostatic and nonelectrostatic solvation effects evaluated using Tomasi's integral equation formalism polarizable continuum model (IEF-PCM), native to Gaussian 03, with applied dielectric constants and a solvent radius corresponding to toluene (ϵ = 2.379, r = 2.82 Å).[19] Thermochemical corrections, determined using the smaller basis set, were applied to the large basis set solvated total energy. Spin density and charge analyses were carried out on converged spin-unrestricted density matrices using the natural population analysis (NPA) method[20] as implemented in NBO 5.0.[21] In a recent study of the oxygenation of an (NHC)$_2$Pd^0 complex, extensive benchmarking calculations were performed to validate our methods for this study.[6d]

Excited electronic states of dioxygen were calculated as solvation-corrected single-point energies using the larger Basis B at the optimized ground-state structure of dioxygen or the PdO_2 adduct. The electronic configuration of converged SCF wavefunctions was confirmed by two methods: first, the value of $\langle S^2 \rangle$, which is ~1.0 for the spin-contaminated open-shell singlet (OSS), 0 for the closed-shell singlet (CSS), and ~2.0 for the open-shell triplet (OST) and second, NBO

(11) Keith, J. M.; Muller, R. P.; Kemp, R. A.; Goldberg, K. I.; Goddard, W. A., III; Oxgaard, J. *Inorg. Chem.* **2006**, *45*, 9631−9633.
(12) A beneficial effect of carboxylic acid additives has been noted in several studies of aerobic palladium oxidation catalysis: (a) Dams, M.; De Vos, D. E.; Celen, S.; Jacobs, P. A. *Angew. Chem., Int. Ed.* **2003**, *42*, 3512−3515. (b) Jensen, D. R.; Schultz, M. J.; Mueller, J. A.; Sigman, M. S. *Angew. Chem., Int. Ed.* **2003**, *42*, 3810−3813. (c) Schultz, M. J.; Hamilton, S. S.; Jensen, D. R.; Sigman, M. S. *J. Org. Chem.* **2005**, *70*, 3343−3352. (d) Rogers, M. M.; Wendlandt, J. E.; Guzei, I. A.; Stahl, S. S. *Org. Lett.* **2006**, *8*, 2257−2260.
(13) Frisch, M. J. et al. *Gaussian 03* (revisions D.01 and B.05); Gaussian Inc.: Pittsburgh, PA, 2004.
(14) Koch, W.; Holthausen, M. C. *A Chemist's Guide to Density Functional Theory*; Wiley-VCH: Weinheim, 2000.
(15) Becke, A. D. *J. Chem. Phys.* **1993**, *98*, 1372−1377.
(16) Lee, C.; Yang, W.; Parr, R. G. *Phys. Rev. B* **1988**, *37*, 785−789.
(17) (a) The Stuttgart RSC 1997 ECP basis set for Pd was obtained from the Extensible Computational Chemistry Environment Basis Set Database, version 02/25/04, as developed and distributed by the Molecular Science Computing Facility, Environmental and Molecular Sciences Laboratory, which is part of the Pacific Northwest Laboratory, P.O. Box 999, Richland, WA 99352 and funded by the U.S. Department of Energy. The Pacific Northwest Laboratory is a multi-program laboratory operated by Battelle Memorial Institute for the U.S. Department of Energy under Contract DE-AC06-76RLO 1830. Contact Karen Schuchardt for further information. (b) Andrae, D.; Häussermann, U.; Dolg, M.; Stoll, H.; Preuss, H. *Theor. Chim. Acta* **1990**, *77*, 123−141.
(18) Hehre, W. J.; Radom, L.; Schleyer, P. v. R.; Pople, J. A. *Ab Initio Molecular Orbital Theory*; Wiley: New York, 1986.
(19) For an overview of solvation models and reviews on PCM methods, see: (a) Cramer, C. J. *Essentials of Computational Chemistry: Theories and Models*; Wiley: New York, 2002. (b) Cramer, C. J.; Truhlar, D. G. *Chem. Rev.* **1999**, *99*, 2161−2200. (c) Tomasi, J.; Mennucci, B.; Cammi, R. *Chem. Rev.* **2005**, *105*, 2999−3093. For references on our current approach, see: (d) Cancès, E.; Mennucci, B.; Tomasi, J. *J. Chem. Phys.* **1997**, *107*, 3032−3041. (e) Mennucci, B.; Tomasi, J. *J. Chem. Phys.* **1997**, *106*, 5151−5158. (f) Mennucci, B.; Cancès, E.; Tomasi, J. *J. Phys. Chem. B* **1997**, *101*, 10506−10517. (g) Tomasi, J.; Mennucci, B.; Cancès, E. *J. Mol. Struct. (Theochem)* **1999**, *464*, 211−226.
(20) Reed, A. E.; Weinstock, R. B.; Weinhold, F. *J. Chem. Phys.* **1985**, *83*, 735−746.
(21) Glendening, E. D.; Badenhoop, J. K.; Reed, A. E.; Carpenter, J. E.; Bohmann, J. A.; Morales, C. M.; Weinhold, F. *NBO 5.0*; Theoretical Chemistry Institute: University of Wisconsin−Madison: Madison, WI, 2001.

spin densities and Lewis structures. When attempting to solve for OSS electronic configurations, it was often necessary to circumvent an automatic basis set projection performed by default in link 401 of G03 (i.e., iop(4/6 = 2)) and in some cases increase the virtual orbital energy gap from the default of 100−400 millihartrees. For spin-corrected OSS total energies ($^1E_{SC}$), spin-projection corrections were applied following the two-state approximation of Yamaguchi et al. (eqs 3 and 4).[22]

$$^1E_{SC} = {}^1E_{UDFT} + f_{SC}[{}^1E_{UDFT} - {}^3E_{UDFT}] \quad (3)$$

$$f_{SC} \approx \frac{{}^1\langle S^2\rangle}{{}^3\langle S^2\rangle - {}^1\langle S^2\rangle} \quad (4)$$

The total electronic energies calculated for the OST and spin-contaminated singlet wavefunctions are denoted by $^3E_{UDFT}$ and $^1E_{UDFT}$, respectively. The fraction of OST spin-contamination in the triplet-contaminated singlet wavefunction is denoted by f_{SC}.

Full and constrained geometry optimizations were carried out in internal coordinates using the default Berny algorithm.[23] Transition states were optimized using standard methods, and intrinsic reaction coordinate (IRC) calculations were performed on the gas-phase transition state to verify that it corresponded to the appropriate reactant/product potential energy surface.[24] IRC results presented in this work include gas-phase total energies calculated at the smaller Basis A without the inclusion of solvation effects.[25] Normal-mode analyses were carried out on the gas-phase optimized ground states and transition states. Zero-point energy, thermal corrections, and entropic corrections were estimated from the normal-mode analysis.

Minimum energy crossing point (MECP) calculations were carried out using Gaussian 98 (G98)[26] following the seam-search method of Harvey with optimization criteria approximately 3 times larger than the default values used within G03.[27] Attempts to apply single-point solvation corrections to the gas-phase optimized MECP for the oxygenation of Pd(0) failed due to the solvation dependence on the geometry at the MECP.[6d] Therefore, Basis A with the IEF-PCM model was used within G98 to optimize the MECP in toluene solvent after which single-point energies with the larger Basis B were calculated within G03. For the HAA pathway, gas-phase optimization of the MECP followed by solvent correction with the larger Basis B was successful and did not necessitate optimization with the solvation model. Normal-mode analyses and the resulting thermochemical corrections were not estimated.

Results and Discussion

Structure of Palladium(II)−Hydride Model Complexes and the Thermodynamics of Their Reaction with Molecular Oxygen. We initiated our study by selecting a model palladium−hydride complex, **14**, that closely resembles the experimental complex $(IMes)_2Pd(H)(O_2CPh)$, **12**. The mesityl substituents of the NHC ligand in **12** were replaced by methyl groups (NHC = IMe),[28] and the benzoate anion was substituted with acetate. To investigate the influence of the ligand trans to the hydride, we also considered complex **15**, *trans*-$(IMe)_2Pd(H)CH_3$, in which the acetate anion in **14** is replaced with a methyl group. This complex is also of interest because it is electronically similar to the (PCP)PdH complex **10** reported by Kemp and Goldberg (eq 1).[9a]

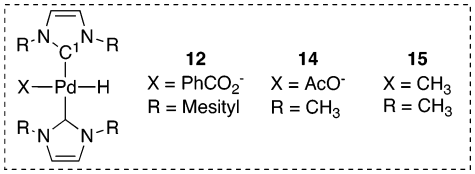

Table 1. Metrical Comparison of Experimental and Computational Pd−H Complexes **12**, **14**, and **15**

	12	**14**	**15**
Pd−H	1.54(2)	1.56	1.65
Pd−X	2.1343(13)	2.18	2.16
Pd−C^1	2.01885(17)	2.05	2.03

The experimental and computational palladium−hydride complexes, **12** and **14**, possess very similar structures (Table 1; see also Figure 1). Substitution of the weak anionic acetate ligand with a methyl group has a significant effect on the *trans*-hydride ligand: the Pd−H bond lengthens from 1.56 Å (**14**) to 1.65 Å (**15**).

The reaction of O_2 with the palladium−hydride complex **14** to form the palladium^{II}−hydroperoxide **16** is calculated to be thermodynamically favorable with a free energy of −14.1 kcal/mol (eq 5). Substitution of the acetate ligand in **14** with a methyl group significantly increases the driving force for reaction of the palladium−hydride with O_2: ΔG° = −26.2 kcal/mol (eq 6).

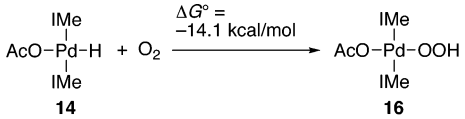

(5)

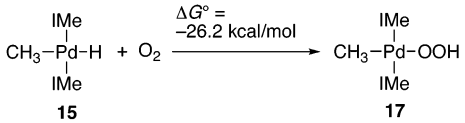

(6)

Mechanism 1: HAA Pathway. Oxygenation of *trans*-$(IMe)_2Pd(H)OAc$, 14. We initiated our study of possible mechanisms for the oxygenation of **14** by probing the interaction of triplet dioxygen with the Pd−H bond and at the axial site of the Pd^{II} center. Efforts to identify a concerted pathway for O_2 insertion into the Pd−H bond were unsuccessful, and no stationary points with a stable Pd−O interaction were identified.[29] In several of these calculations, we noted that the dioxygen molecule moved away from the axial position during the optimization, toward the hydride ligand. Subsequent analysis

(22) Our use of spin-projection corrections was previously discussed in the Supporting Information of ref 6a. For additional references, see: (a) Yamaguchi, K.; Jensen, F.; Dorigo, A.; Houk, K. N. *Chem. Phys. Lett.* **1988**, *149*, 537−542. (b) Yamanaka, S.; Kawakami, T.; Nagao, H.; Yamaguchi, K. *Chem. Phys. Lett.* **1994**, *231*, 25−33.

(23) (a) Peng, C.; Ayala, P. Y.; Schlegel, H. B.; Frisch, M. J. *J. Comput. Chem.* **1996**, *17*, 49−56. (b) Peng, C.; Schlegel, H. B. *Isr. J. Chem.* **1993**, *33*, 449−454.

(24) (a) Gonzalez, C.; Schlegel, H. B. *J. Chem. Phys.* **1989**, *90*, 2154−2161. (b) Gonzalez, C.; Schlegel, H. B. *J. Chem. Phys.* **1990**, *94*, 5523−5527.

(25) In a recent study of the oxygenation of an $(NHC)_2Pd^0$ complex (ref 6d), we compared the results of gas-phase- and implicit toluene optimized (IEF-PCM) stationary-point calculations. We found that the relative total energies varied by less than 1 kcal/mol between the optimization methods, and the stationary-point geometries changed very little upon inclusion of the implicit solvation model. Therefore, we expect that implicit toluene solvation will have little effect on the gas-phase IRC results presented in this study.

(26) Frisch, M. J. et al. *Gaussian 98* (revision A.9); Gaussian, Inc.: Pittsburgh, PA, 2001.

(27) Harvey, J. N.; Aschi, M.; Schwarz, H.; Koch, W. *Theor. Chem. Acc.* **1998**, *99*, 95−99.

(28) Benchmarking calculations comparing the energies of Pd complexes bearing IMe and full IMes ligand were performed, and the results suggest that substitution of IMes with IMe has only a small impact on the relative energies (±1−4 kcal/mol). See Supporting Information Figure S1.

(29) These results are consistent with previous studies by Goddard and co-workers in which they examined other possible dioxygen insertion pathways without success, see: refs 8b and 11.

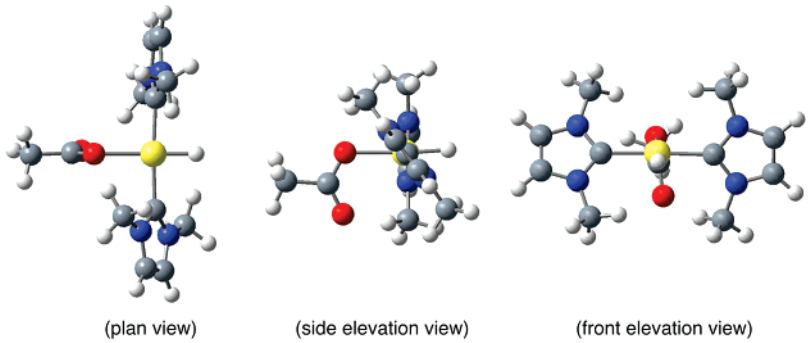

Figure 1. Ball-and-stick models of the gas-phase optimized structure of $(IMe)_2Pd(H)(OAc)$, **14**.

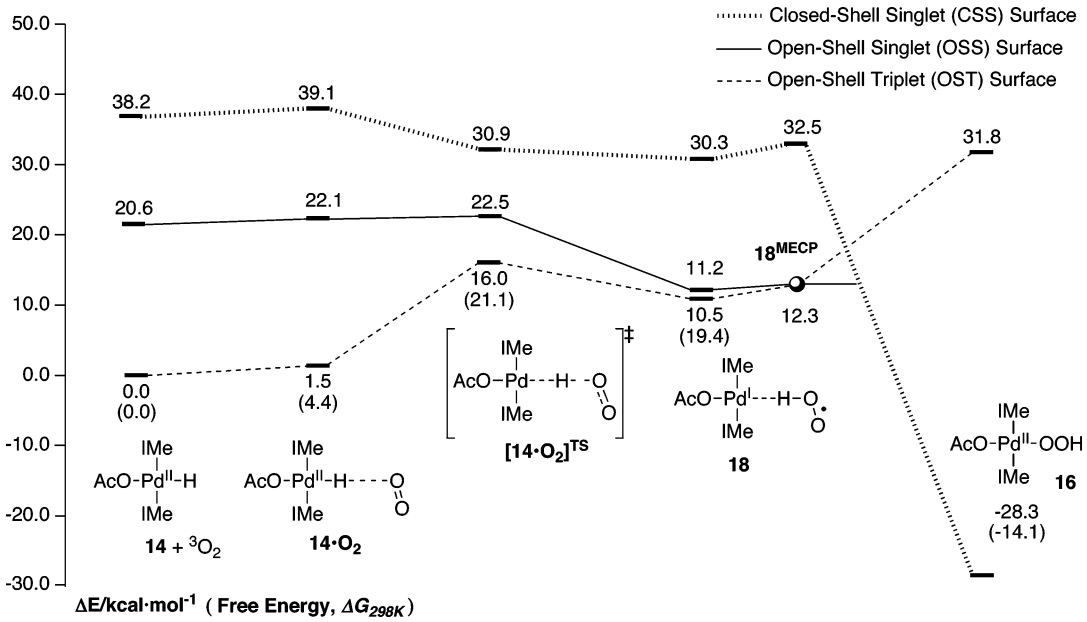

Figure 2. Reaction profile for hydrogen atom abstraction from $(IMe)_2Pd(H)(OAc)$, **14**, by molecular oxygen to form $(IMe)_2Pd(OOH)(OAc)$, **16**.

revealed the formation of a weak adduct between **14** and molecular oxygen, **14·O₂**, in which the O_2 molecule is approximately 5 Å from the Pd center along the Pd−H vector. The geometry of this adduct, which is similar to adducts reported by Goddard and co-workers in their study of reactions between other palladium−hydride complexes and dioxygen (e.g., Scheme 4),[8b,11] prompted us to evaluate the energetics of a HAA mechanism for O_2 insertion into the Pd−H bond of **14**.

The O_2 fragment retains a bent, end-on orientation with respect to the Pd−H bond as dioxygen approaches closer to the Pd center. At a Pd−O distance of 3.01 Å, a transition state was located for abstraction of the hydrogen atom by dioxygen, **[14·O₂]^{TS}**, which has a free energy 21.1 kcal/mol higher than the separated reagents (Figure 2). This HAA step generates a protonated superoxide species coordinated to a T-shaped Pd^I center via a weak Pd···H interaction (**18**). The open-shell triplet (OST) electronic state is lower in energy than the open-shell singlet and closed-shell singlet (OSS and CSS) states through intermediate **18** on the reaction coordinate. At intermediate **18**, the energies of the OST and OSS states converge. The similar energies of the OST and OSS states of **18** reflect the lack of electronic communication between the unpaired electrons, which are spatially separated on the Pd and HOO fragments. We utilized the seam-search method of Harvey and co-workers to locate the MECP between the triplet and the singlet spin surfaces beyond intermediate **18**.[27] The optimized structure of **18^{MECP}** is only slightly higher in energy (12.3 kcal/mol) than the preceding intermediates **^{3}18** and **^{1}18** (10.5 and 11.2 kcal/mol, respectively). The palladium−hydroperoxide product **16** is formed by rotation of the HOO fragment and formation of the Pd−O bond.

The optimized O−O bond length in **14·O₂** is nearly the same as that of free O_2, indicating that essentially no charge transfer has occurred to the dioxygen molecule (Figure 3). A similar conclusion is supported by natural spin density (NSD) analysis, which indicates that all of the unpaired spin density in **14·O₂** lies on the dioxygen fragment. The hydride ligand at the transition state is calculated to be 1.76 Å from the Pd center and 1.25 Å from the O_2 fragment (Figure 3). Natural charge (NC) analysis indicates that the hydride ligand in **14** possesses weak hydridic character, namely, it bears an anionic charge ($NC_H = -0.181$). As dioxygen approaches, the hydride ligand acquires increasingly protic character, and at the transition state **[14·O₂]^{TS}**, it bears a NC of +0.208. The O−O bond at the transition state is elongated to 1.28 Å, consistent with partial electron transfer to the O_2 fragment. NSD analysis reveals that the majority of unpaired spin density resides on O_2 and is distributed approximately equally over both oxygen atoms ($O_\alpha = 0.631$ and $O_\beta = 0.743$). The remaining spin density resides

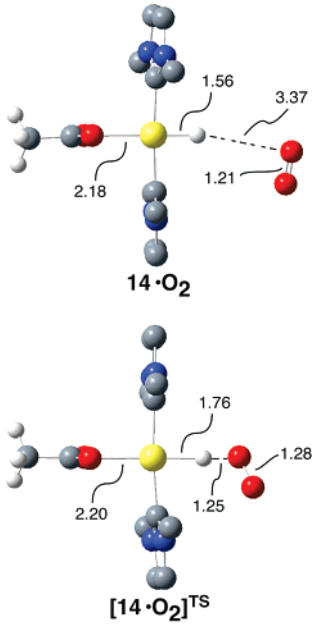

Figure 3. Ball-and-stick structures and metrics of the calculated palladium−dioxygen species **14·O$_2$** and **[14·O$_2$]^{TS}**.

primarily on Pd (0.376), H (0.035), and the coordinated oxygen atom of the acetate ligand (0.112).

Further reduction of O_2 is evident in intermediate **18**, which features an O−O bond length of 1.33 Å (Figure 4), very similar to the experimentally derived bond length of free protonated superoxide (1.30 Å).[30] The natural charge on the hydrogen atom bridging Pd and the O_2 fragment in **18** is substantially protic ($NC_H = +0.420$), and the O_α−H bond length has shortened to 1.02 Å. The NSD on the Pd center is 0.637, which is nearly double that of the transition-state structure **[14·O$_2$]^{TS}** (0.376). The spin density on the superoxide fragment lies primarily on the remote (β) oxygen atom ($O_\alpha = 0.345$ and $O_\beta = 0.705$). These characteristics are consistent with the formulation of **18** as a Pd^{I} adduct of protonated superoxide. The properties of **18^{MECP}** are nearly identical to those of **18** (Figure 4).

We were unable to identify the precise pathway for rearrangement of the HOO fragment in the conversion of **18^{MECP}** into **16**.[31] We initially postulated that an electron pair on the Pd center could act as the H-bond acceptor and provide a hinge for rotation of the HOO species; however, constrained geometry optimizations indicated that the energies associated with such a rearrangement were too high to be relevant. Complete dissociation of the HOO fragment from the Pd^{I} center appears to be energetically accessible, with a free energy of ~6 kcal/mol lower than that of **[14·O$_2$]^{TS}** (eq 7). This step represents a possible initiation step for radical-chain autoxidation of the Pd−H species, a pathway that has been detected in the oxygenation of other metal−hydrides.[32] Experimental studies of the oxygenation of **10** and **12**, however, indicate that these reactions do not proceed by a radical-chain mechanism. Consequently, if the HAA pathway is operating in the oxygenation of these complexes, rearrangement of the HOO fragment to form the Pd−OOH complex must occur without release of radicals into bulk solution. For example, the fragments could separate and rearrange within a solvent cage.

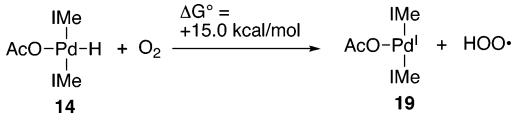

(7)

Oxygenation of *trans*-(IMe)$_2$Pd(H)(CH$_3$), 15. Recent calculations by Goddard et al. suggested that the oxygenation of the (PCP)Pd(H) complex **10** proceeds by the HAA pathway. The palladium−hydride complexes **10** and **12** (eqs 1 and 2) are structurally similar, but the anionic ligands trans to the hydride are quite different: the aryl ligand in **10** is a strong sigma donor, whereas the acetate ligand in **12** is a weak donor ligand. The results shown in eqs 5 and 6 revealed that replacement of the *trans*-acetate ligand in **14** with a methyl group increases the thermodynamic driving force for O_2 insertion by more than 12 kcal/mol. The presence of a strong donor ligand trans to the hydride also lowers the kinetic barrier for abstraction of a hydrogen atom by O_2. Calculations analogous to those described previously for the reaction of **14** with O_2 (Figure 2) were performed to evaluate the oxygenation of **15**. The transition state, **[15·O$_2$]^{TS}**, which has a structure very similar to **[14·O$_2$]^{TS}**, has an elongated Pd−H distance of 1.80 Å (eq 8). The calculated free energy of activation for eq 8, 14.7 kcal/mol, is 6.4 kcal/mol lower in energy than for the oxygenation of **14**. This markedly lower activation barrier is attributed to the greater electron-donating ability of the methyl ligand relative to acetate, a property that increases the hydridic character of the palladium−hydride ($NC_H = -0.378$) and facilitates reduction of molecular oxygen.

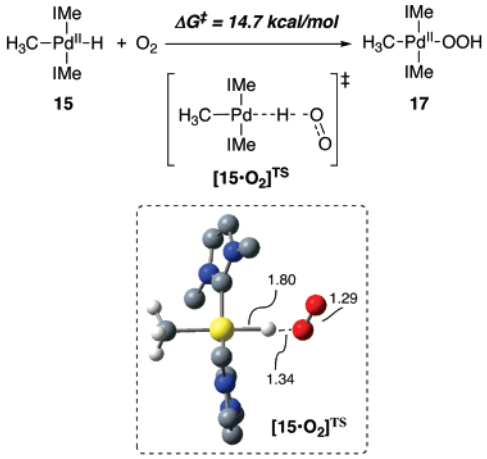

(8)

Mechanism 2: HX Reductive Elimination Pathway. Thermodynamic Analysis and Experimental Considerations. The traditional mechanism for catalyst reoxidation in Pd-catalyzed aerobic oxidation reactions involves the oxygenation of a Pd^{0} center that arises from reductive elimination of HX from a palladium^{II}−hydride species (Scheme 2). The experimental study of the oxygenation of (IMes)$_2$Pd(H)(O$_2$CPh) (**12**) (eq 2) provided no evidence for intermediates in the reaction, but the data cannot exclude a stepwise mechanism initiated by

(30) Smith, D. W.; Andrews, L. *J. Chem. Phys.* **1974**, *60*, 81−85.
(31) In the computational study of the oxygenation of **12** (ref 11), Goddard et al. indicate that the HOO fragment rotates to allow for triplet−singlet surface crossing and formation of the Pd−O bond. However, the energetics or structural requirements for such a rearrangement are not described.
(32) (a) Endicott, J. F.; Wong, C.-L.; Inoue, T.; Natarajan, P. *Inorg. Chem.* **1979**, *18*, 450−454. (b) Bakac, A. *J. Am. Chem. Soc.* **1997**, *119*, 10726−10731. (c) Bakac, A. *J. Photochem. Photobiol. A: Chem.* **2000**, *132*, 87−89. (d) Wenzel, T. T. *Stud. Surf. Sci. Catal.* **1991**, *66*, 545−554. (e) Wick, D. D.; Goldberg, K. I. *J. Am. Chem. Soc.* **1999**, *121*, 11900−11901.

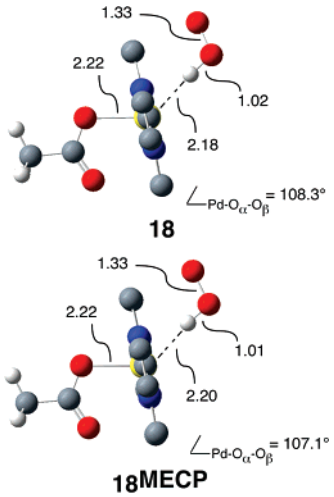

Figure 4. Ball-and-stick structures and metrics of the calculated palladium−dioxygen species **18** and **18**^{MECP}.

reductive elimination of carboxylic acid: **B** → **C** → **D** → **E** in Scheme 2. To probe this possible pathway, we performed DFT calculations on each of the three steps in the sequence: (1) reductive elimination of HOAc from *trans*-(IMe)$_2$Pd(H)OAc (**14**), (2) oxygenation of (IMe)$_2$Pd^0 (**20**), and (3) protonolysis of a Pd−O bond of (IMe)$_2$Pd(η^2-O$_2$) (**21**). The calculations reveal that each of these three steps is thermodynamically favorable in toluene (eqs 9−11).

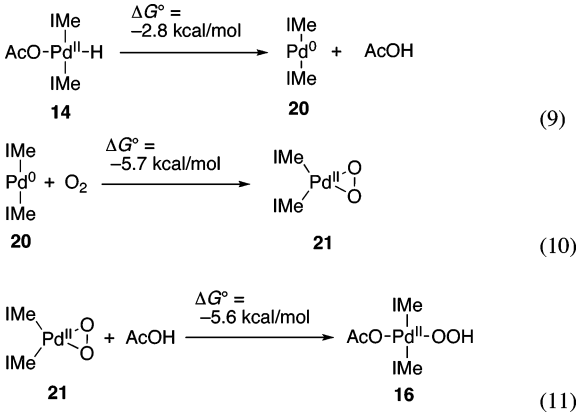

Reactions analogous to eqs 10 and 11 have been studied experimentally with Pd complexes bearing IMes ligands,[2b] and the results reveal that oxygenation of (IMes)$_2$Pd^0 and protonolysis of a Pd−O bond of (IMes)$_2$Pd(η^2-O$_2$) by acetic acid are kinetically quite facile. These two reactions proceed essentially instantaneously when the reagents are combined in solution at −78 °C and at room temperature, respectively. No experimental data are currently available for the reductive elimination of HOAc from (IMes)$_2$Pd(H)(O$_2$CR) complexes (eq 9); however, reversible formation of palladium−hydrides has been identified in other systems.[5] These experimental results together with the favorable thermodynamics for eqs 9−11 suggest that the three-step HX reductive elimination pathway is a viable mechanism for palladium−hydride oxygenation. Therefore, additional DFT calculations were performed to probe the kinetic barriers and gain fundamental insights into the mechanism of each of the steps in the sequence.

Reductive Elimination of AcOH from *trans*-(IMe)$_2$Pd(H)-OAc, 14. We envisioned two possible mechanisms for reductive elimination of AcOH from **14**: (1) a stepwise pathway involving ionization of the acetate ligand followed by acetate deprotonation of the cationic palladium−hydride complex and (2) a single-step pathway involving concerted O−H bond formation via a metallacyclic transition state.

Analysis of the thermodynamics of the two steps in the first pathway reveals that acetate ionization in toluene to form the solvent-separated Pd^{II} cation (**22**) and acetate anion is uphill by 37 kcal/mol (eq 12). Deprotonation of the hydride in **22** by acetate forms a product best described as a hydrogen-bonded acetic acid adduct of Pd^0 complex **20** (eq 13). The latter step is very favorable thermodynamically ($\Delta G° = -33.6$ kcal/mol), and constrained geometry and transition-state optimization calculations reveal that the reaction proceeds without a barrier. Despite the facile second step of this sequence, the large energy cost associated with ionization of the acetate ligand suggests that this mechanism is improbable in a nonpolar solvent such as toluene.

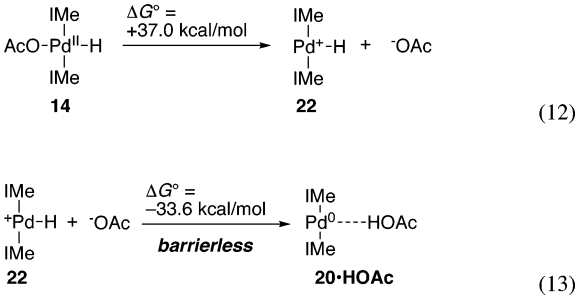

Concerted reductive elimination of acetic acid from **14** could proceed by a three- or five-membered metallacyclic transition state, **23** or **24**, respectively. These possibilities were examined by performing constrained potential energy surface scans on the oxidative addition of AcOH to the Pd^0 center in **20**, namely, the microscopic reverse of AcOH reductive elimination. Initial calculations revealed that the energy of the five-membered pathway is lower than the three-membered pathway, and a transition-state structure with a single imaginary frequency was located for the five-membered pathway. Intrinsic reaction coordinate (IRC) calculations confirmed that the transition state is connected to both the reactant and the product, **14** and **20·HOAc**, respectively (Figure 5).

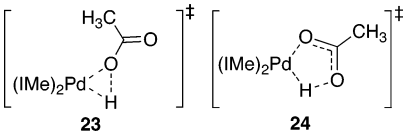

Analysis of the structures along this reaction coordinate (Figure 5) reveals that the concerted reductive elimination of AcOH proceeds by rotation of the acetate and hydride ligands about the IMe−Pd−IMe axis. The H−Pd−O angle in the initial palladium^{II}−hydride complex **14** is 175.6°, whereas at the transition state, this angle diminishes to 86.9°. This motion of the acetate and hydride ligands brings them into spatial proximity and enables the distal (γ) oxygen atom of acetate to establish a bonding interaction with the hydride ligand. The

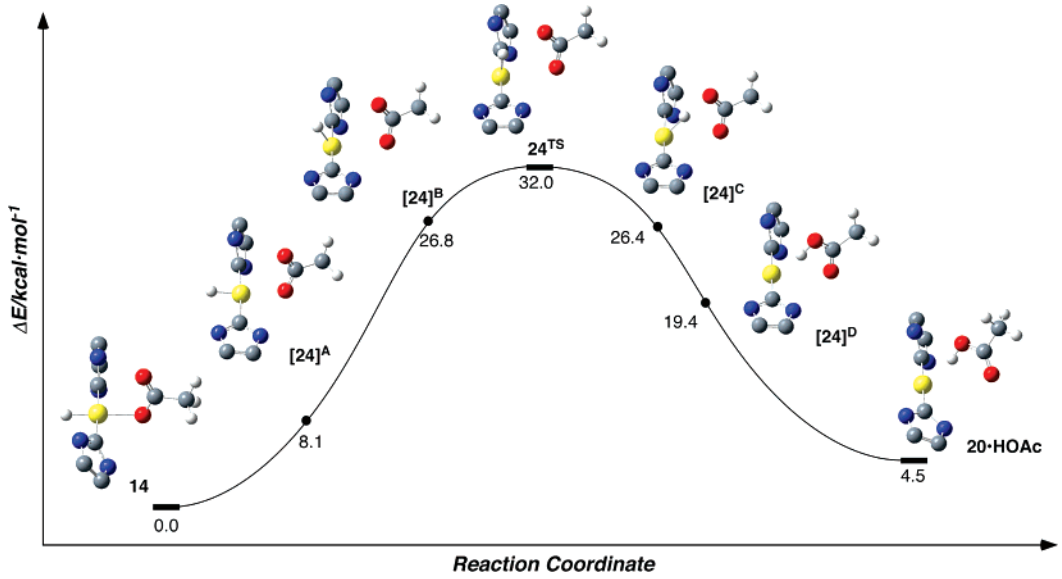

Figure 5. Intrinsic reaction coordinate results for the reductive elimination of AcOH from the Pd−H complex **14** defined by transition state **24**^{TS} with total energies in kcal/mol. The H atoms and *N*-methyl substituents of the IMe ancillary ligands have been omitted for clarity.

activation barrier ($\Delta G^{\ddagger}$) for reductive elimination of AcOH from **14** is 25.9 kcal/mol (eq 14).

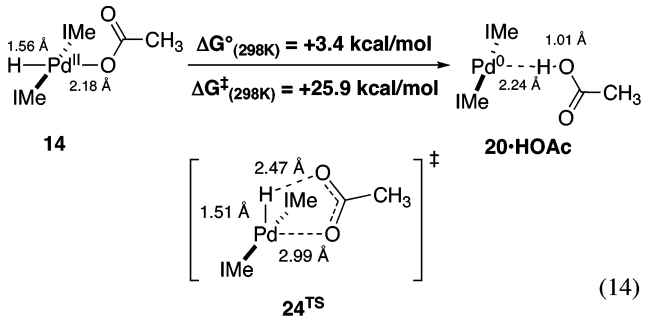

(14)

Significant elongation of the Pd−O bond occurs along the reaction coordinate, proceeding from 2.18 Å in **14** to 2.99 Å in **24**^{TS}. The Pd−O and O−H bonds in **24**^{TS} are sufficiently long that this structure can be described as an electrostatic complex between acetate and the palladium−hydride cation **22**. In support of this designation, the Pd−H bond length in the transition state (1.51 Å) is shorter than that in **14** (1.56 Å) and nearly identical to the Pd−H bond length of the T-shaped palladium−hydride cation **22** (1.52 Å). Furthermore, natural charge calculations reveal that the acetate fragment in **24**^{TS} bears nearly a full unit of anionic charge, −0.92. These observations suggest that the concerted reductive elimination pathway possesses significant ionic character; however, it avoids the energetic cost of charge separation in a nonpolar solvent that occurs in the stepwise mechanism in eqs 12 and 13.

Considerable recent work implicates carboxylate ligands coordinated to Pd^{II} as internal Brønsted bases in various chemical processes, including the formation of palladium^{II}−alkoxides in alcohol oxidation reactions,[4] palladation of arene C−H bonds,[33] and a novel proposed reductive β-hydride elimination involving palladium^{II}−alkoxides.[6c] Similarly, the concerted reductive elimination of AcOH in eq 14 can be viewed as an intramolecular deprotonation of the palladium−hydride by the acetate ligand.

Oxygenation of (IMe)$_2$Pd^0, 20. We recently reported a full DFT analysis of the reaction of molecular oxygen with Pd^0 complex **20**;[6d] the key results will be summarized here (Figure 6). The initial reaction between molecular oxygen and the Pd^0 center in **20** forms an η^1-O_2 adduct, **23**, in which the IMe ligands retain a trans configuration. Ligand isomerization from the trans to cis configuration proceeds through transition state **25**^{TS} to generate the isomeric η^1-O_2 adduct, **26**. The O−O bond length in **26**, 1.30 Å, suggests that this complex is best described as a Pd^{I}−(η^1-superoxide) species. Prior to formation of **26**, the open-shell singlet and closed-shell singlet electronic configurations are considerably higher in energy than the open-shell triplet configuration. At the geometry of **26**, however, the three spin states are separated by only 2.4 kcal/mol. The MECP was calculated, and the structure at this point, **26**^{MECP}, exhibits a geometry very similar to **26**. Beyond the MECP, the closed-shell singlet η^2-peroxo product **21** forms without a barrier. The highest energy point observed along the reaction coordinate is transition state **25**^{TS}, which has a free energy only 9.6 kcal/mol higher than the separated reagents, **20** + O_2.

Protonolysis of (IMe)$_2$Pd(η^2-O$_2$), 21. The third and final step of the HX reductive-elimination pathway for palladium−hydride oxygenation is protonolysis of a Pd−O bond of the η^2-peroxo complex (eq 11). The calculations reveal that a weak, hydrogen-bond adduct, **21·HOAc**, forms between the peroxo−Pd^{II} complex **21** and acetic acid, a species stabilized by 1.6 kcal/mol relative to the separated reactants (eq 15).

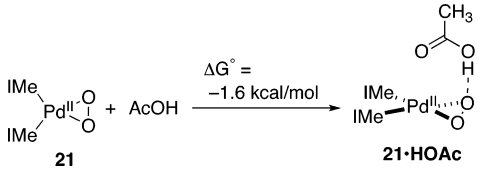

(15)

Potential energy surface scans led to the identification of a transition state for the conversion of **21·HOAc** into the palladium−hydroperoxide product **16** (Figure 7). Analysis of

(33) (a) Davies, D. L.; Donald, S. M. A.; Macgregor, S. A. *J. Am. Chem. Soc.* **2005**, *127*, 13754−13755. (b) Lafrance, M.; Fagnou, K. *J. Am. Chem. Soc.* **2006**, *128*, 16496−16497.

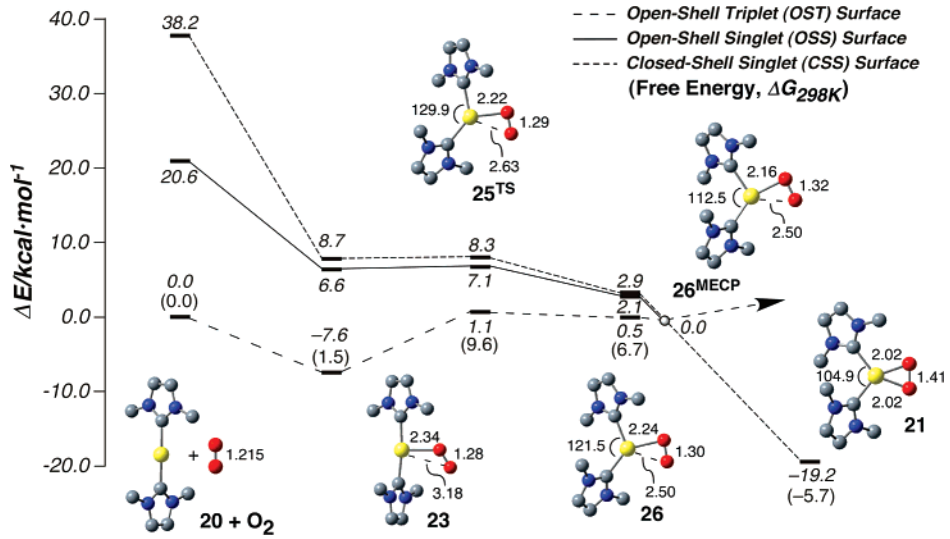

Figure 6. Reaction coordinate for the oxygenation of $(IMe)_2Pd(0)$, **14**, with notable bond lengths (Å) and angles (deg).

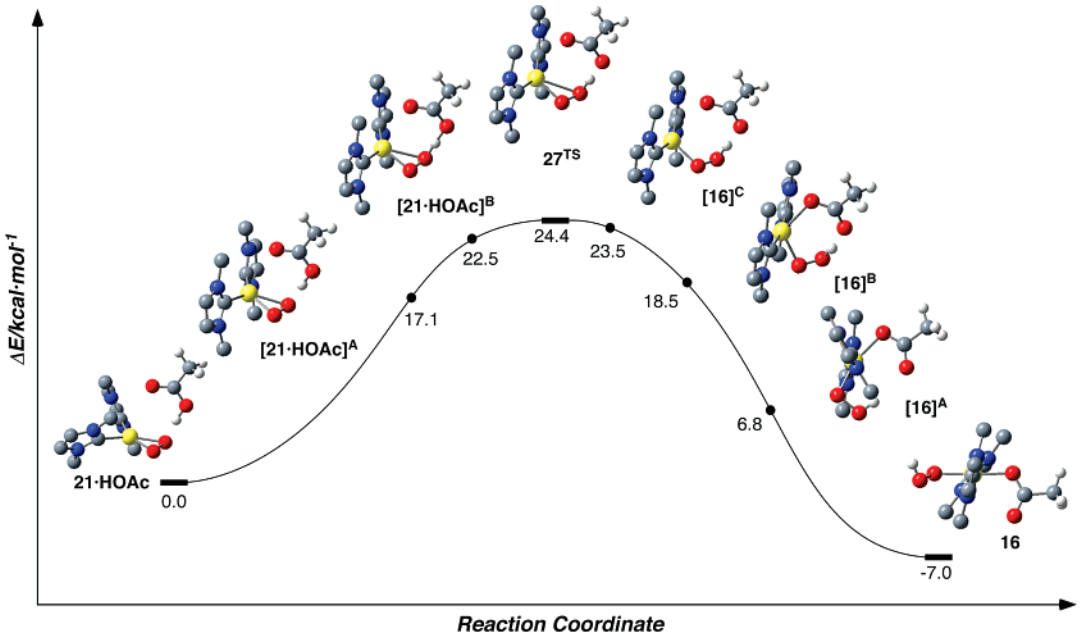

Figure 7. Intrinsic reaction coordinate for the protonation of **21** defined by transition state $\mathbf{27}^{TS}$ with total energies in kcal/mol.

the intrinsic reaction coordinate that connects transition state $\mathbf{27}^{TS}$ with **21·HOAc** and **16** reveals that Pd−O bond protonolysis proceeds in concert with cis−trans isomerization of the IMe ligands and coordination of the acetate to the Pd center (Figure 7). Proton transfer from acetic acid to a peroxo oxygen atom formally occurs prior to the transition state, and the transition-state structure is best described as a Pd^{II}(OOH) species with an acetate anion hydrogen bonded to the hydroperoxo moiety. The angle between the IMe ligands in $\mathbf{27}^{TS}$ ($\angle_{C-Pd-C}$ = 151.3°) has widened considerably relative to that in **21·HOAc** (99.7°), approaching a trans configuration. Beyond the transition state, the distal oxygen atom of acetate interacts with the Pd^{II} center from the axial direction, and the OOH fragment shifts downward toward the opposite axial face (see $\mathbf{[16]}^{B}$, Figure 7). This motion enables the protonolysis step to proceed directly to the trans configuration of the $(IMe)_2Pd(OOH)OAc$ complex.

Overall Mechanism for the HX Reductive Elimination Pathway. In Figure 12, we show the complete energy diagram for oxygenation of the palladium−hydride complex **14** via the HX reductive elimination pathway. Inspection of the reaction coordinate reveals that reductive elimination of AcOH from **14** is the rate-limiting step in the overall transformation. Subsequent oxygenation of Pd^0 complex **20** exhibits a much lower barrier. Thus, upon reductive elimination of AcOH from the palladium−hydride complex **14**, Pd^0 will be trapped rapidly by O_2 to form the η^2-peroxo adduct **21**. The competing oxidative addition of AcOH to **20**, which regenerates the palladium−hydride species, possesses a much higher barrier.

The free energy barrier for protonolysis of the η^2-peroxo−palladium(II) adduct **21**, which proceeds through the acetic acid adduct **21·HOAc**, is comparable to that of AcOH reductive elimination, 26.1 and 25.9 kcal/mol, respectively. Although this difference is within the error limits of the present calculations, estimated to be ±3−5 kcal/mol, it suggests that an η^2-peroxo species might build up to a detectable level during the palladium−hydride oxygenation. No such evidence for an η^2-peroxo species was obtained in our previously published

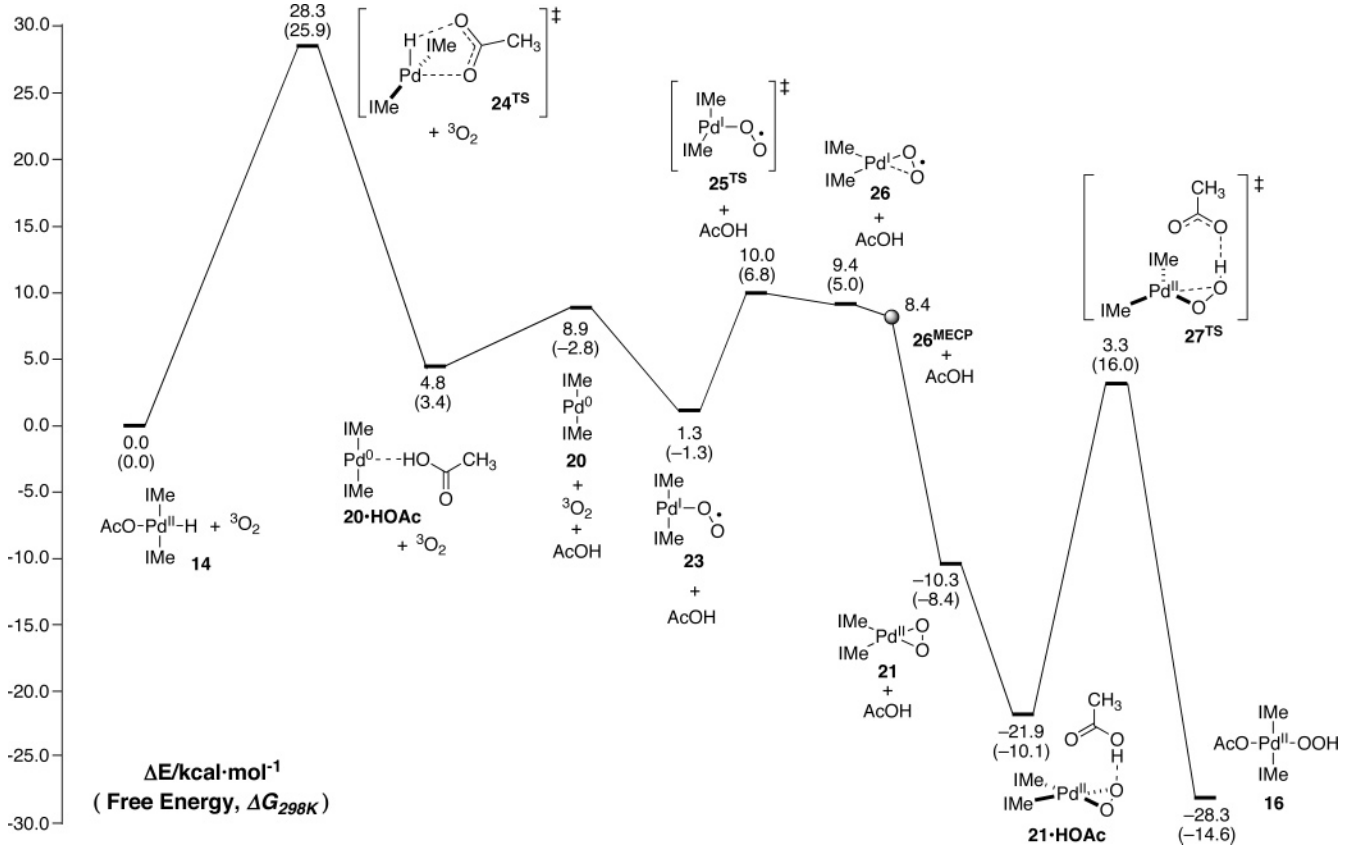

Figure 8. Complete energy profile for palladium−hydride oxygenation pathway involving AcOH reductive elimination/Pd^0 oxygenation/AcOH protonolysis of $Pd(\eta^2\text{-}O_2)$.

experimental studies;[9b] however, in more recent studies, we have detected small amounts of the η^2-peroxo species under certain reaction conditions. These experimental observations will be elaborated in a forthcoming full paper focused on the mechanism of the oxygenation of **12**.[34]

Mechanism 3: Peroxo−Pd^{IV} Pathway. Molecular oxygen reacts with a number of late transition-metal complexes to form η^2-peroxo adducts.[2,35,36] One of the earliest and most prominent examples of this reactivity is the oxygenation of Vaska's complex (eq 16).[35b,37] The isoelectronic relationship between square-planar Pd^{II} complexes and Vaska's complex suggests the oxygenation of palladium−hydride complex **14** could be initiated by oxidative addition of O_2 to the Pd^{II} center. Subsequent reductive elimination of an O−H bond will generate the palladium^{II}−hydroperoxide product (Scheme 5, mechanism 3). No experimental precedent exists for η^2-peroxo−Pd^{IV} species; however, the oxidative addition of O_2 to **14** might be facilitated by the presence of strong donor ligands coordinated to Pd^{II} (two NHCs and a hydride).

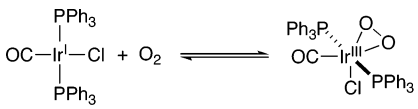

(16)

A stable ground-state structure was identified for the η^2-peroxo−Pd^{IV} complex $(IMe)_2Pd(O_2)(H)(OAc)$ (**28**). The O−O bond length in **28**, 1.39 Å (Figure 9), is shorter than the O−O

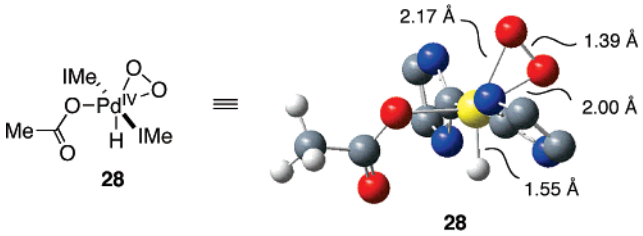

Figure 9. Ball-and-stick representation and key bond lengths for the calculated structure of $(IMe)_2Pd^{IV}(O_2)(H)(OAc)$ (**28**).

bond length calculated for the η^2-peroxo−Pd^{II} complex $(IMe)_2Pd(O_2)$ (**21**), 1.41 Å, consistent with the expectation that the Pd^{II} center in **21** is capable of greater charge transfer (back-bonding) to the O_2 fragment than the Pd^{IV} center in **28**. The two Pd−O bond lengths to the peroxo ligand in **28** are substantially different, 2.00 and 2.17 Å, and as expected, the longer bond is opposite the hydride ligand, which exhibits a strong trans influence.

The calculated free energy ($\Delta G°$) for formation of the η^2-peroxo−Pd^{IV} complex, +35 kcal/mol (eq 17), is substantially higher than even the activation barriers ($\Delta G^{‡}$) associated with the previous two pathways for palladium−hydride oxygenation

(34) Konnick, M. M.; Stahl, S. S., unpublished results.
(35) For early examples, see: (a) Valentine, J. S. *Chem. Rev.* **1973**, *73*, 235−245. (b) Vaska, L. *Acc. Chem. Res.* **1976**, *9*, 175−183.
(36) For recent examples, see: (a) Aboelella, N. W.; Kryatov, S. V.; Gherman, B. F.; Brennessel, W. W.; Young, V. G., Jr.; Sarangi, R.; Rybak-Akimova, E. V.; Hodgson, K. O.; Hedman, B.; Solomon, E. I.; Cramer, C. J.; Tolman, W. B. *J. Am. Chem. Soc.* **2004**, *126*, 16896−16911. (b) Lanci, M. P.; Brinkley, D. W.; Stone, K. L.; Smirnov, V. V.; Roth, J. P. *Angew. Chem., Int. Ed.* **2005**, *44*, 7273−7276. (c) Smirnov, V. V.; Brinkley, D. W.; Lanci, M. P.; Karlin, K. D.; Roth, J. P. *J. Mol. Catal. A: Chem.* **2006**, *251*, 100−107.
(37) (a) Vaska, L. *Science* **1963**, *140*, 809−810. (b) Vaska, L.; Chen, L. S.; Senoff, C. V. *Science* **1971**, *174*, 587−589.

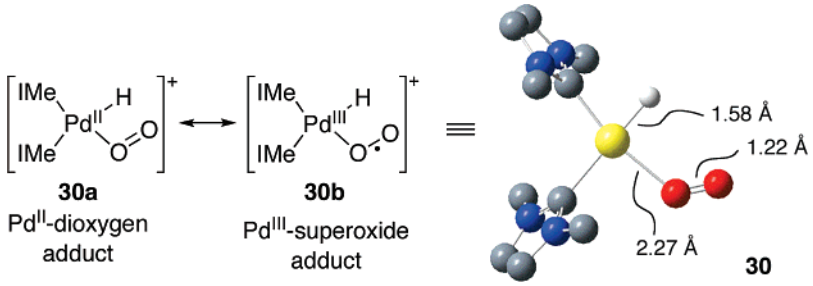

Figure 10. Ball-and-stick representation and key bond lengths for the calculated structure of $(IMe)_2Pd(H)(O_2)$ (**30**).

(HAA and HX reductive elimination). If the acetate ligand is replaced with a more strongly donating methyl group, the η^2-peroxo−Pd^{IV} species is significantly more stable (eq 18). Nevertheless, the acetate-for-methyl ligand exchange also dramatically lowers the barrier for the hydrogen atom abstraction mechanism ($\Delta G^{\ddagger} = 14.7$ kcal/mol; eq 8). Thus, the Pd^{IV} pathway for palladium−hydride oxygenation appears to be energetically prohibitive for both palladium−hydride species **14** and **15**.

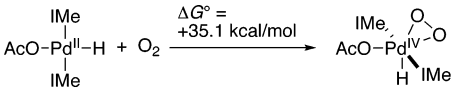

(17)

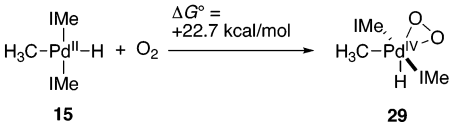

(18)

Mechanism 4: O_2 Insertion Pathway. The final mechanism that we evaluated for palladium−hydride oxygenation, the O_2 insertion pathway, is so named because the mechanism most closely resembles an insertion of O_2 into a Pd−H bond. Although efforts to identify concerted mechanisms for insertion of O_2 into the Pd−H bond of **14** have been unsuccessful, a ground-state structure was calculated for a triplet η^1-O_2 adduct, *cis*-$(IMe)_2Pd(H)(O_2)$ (**30**). The short O−O bond in **30** (1.22 Å), which is only minimally perturbed from the bond length in molecular oxygen (1.21 Å), suggests that this structure constitutes a weak dioxygen adduct of Pd^{II} rather than a palladium^{III}−superoxide species (Figure 10). Namely, minimal Pd → O_2 charge transfer is evident in **30** (as might be expected for a cationic Pd^{II} center).

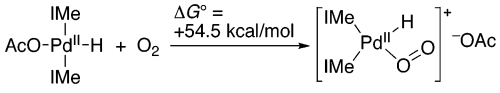

(19)

A possible mechanism for the formation of **30** involves dissociation of acetate, trans-to-cis isomerization of the IMe ligands, and O_2 coordination to the Pd center (Scheme 5, mechanism 4). This species is not a likely intermediate in the oxygenation of palladium−hydride **14**, however, because its ground-state free energy is 54.5 kcal/mol higher than that of **14** + O_2. Indeed, this pathway appears to be the least favorable of all of the mechanisms considered. The origin of the unfavorable energy for this pathway is at least two-fold: (1) charge separation in a nonpolar solvent is highly unfavorable and (2) the cationic Pd^{II} center is a poor reducing agent and, therefore, forms only a weak adduct with O_2. Furthermore, the results presented previously suggest that, if the acetate ligand dissociates, it can react with the cationic palladium−hydride without a barrier to produce AcOH and Pd^0 (eq 13).

Effect of Exogenous Carboxylic Acid on Palladium−Hydride Oxygenation Pathways. The preceding systematic analysis of the four palladium−hydride oxygenation pathways proposed in Scheme 5 reveals that two of the mechanisms, hydrogen atom abstraction and HX reductive elimination, exhibit similar free energies of activation, $\Delta G^{\ddagger} = 21.1$ and 25.9 kcal/mol, respectively. Both of these values compare favorably with the experimental activation energy, $\Delta G^{\ddagger} = 24.4(5)$ kcal/mol.[38] The intrinsic uncertainties associated with DFT calculations, particularly when comparing two fundamentally different chemical processes (i.e., homolytic vs heterolytic bond formation and cleavage), suggest that these two mechanisms are essentially isoenergetic. Thus, the preferred mechanism cannot be determined solely on the basis of the calculated activation barriers.

When the present computational study was initiated, relatively little experimental data were available to facilitate distinction between possible mechanisms for palladium−hydride oxygenation; however, one unusual observation in the original experimental study of the oxygenation of palladium−hydride complex **12** (eq 2) was the beneficial effect of carboxylic acid on the reaction rate. Therefore, we performed additional DFT calculations to probe the potential influence of explicit carboxylic acid on the hydrogen atom abstraction and HX reductive elimination pathways.

We began this study by examining the ground-state interaction between acetic acid and palladium−hydride complex **14**. An adduct was found, **14·HOAc** (eq 20), which features a stabilizing hydrogen-bonding interaction between acetic acid and the carbonyl oxygen atom of the acetate ligand ($\Delta E° = -4.5$ kcal/mol).[39,40]

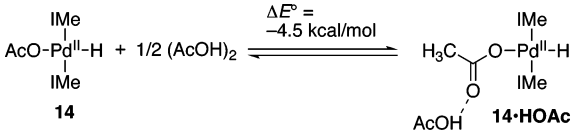

(20)

Formation of **14·HOAc** has a slight inhibitory effect on the HAA mechanism; namely, a higher activation barrier is observed

(38) This activation barrier is derived from the experimental rate constant (2.21×10^{-4} s^{-1}) for the oxygenation of **12** in benzene at 51 °C (see ref 10).
(39) This structure rationalizes the experimental observation that addition of benzoic acid to a solution of the palladium−hydride complex **12** in benzene or toluene causes the resonances of the coordinated benzoate ligand to broaden in the ^1H NMR spectrum. The extent of broadening increases with increased concentrations of added benzoic acid.

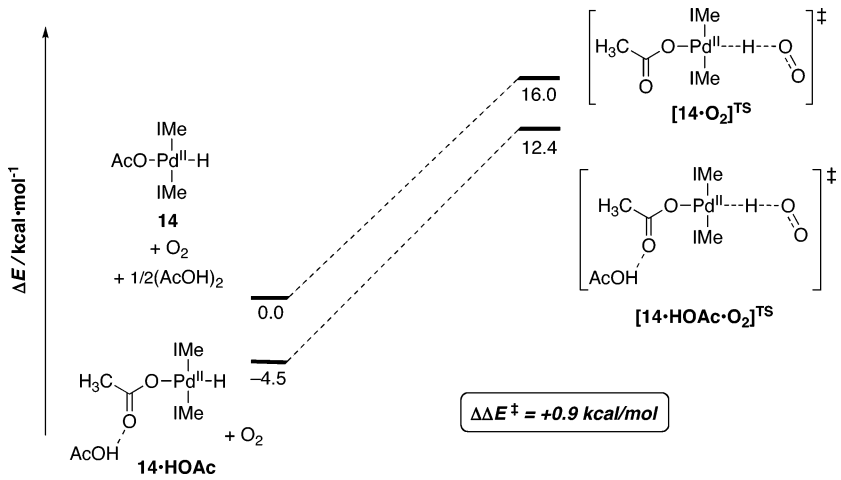

Figure 11. Influence of exogenous AcOH on the energy barrier ($DE^{\ddagger}$) for hydrogen atom abstraction from $(IMe)_2Pd(H)(OAc)$, **14**, by molecular oxygen.

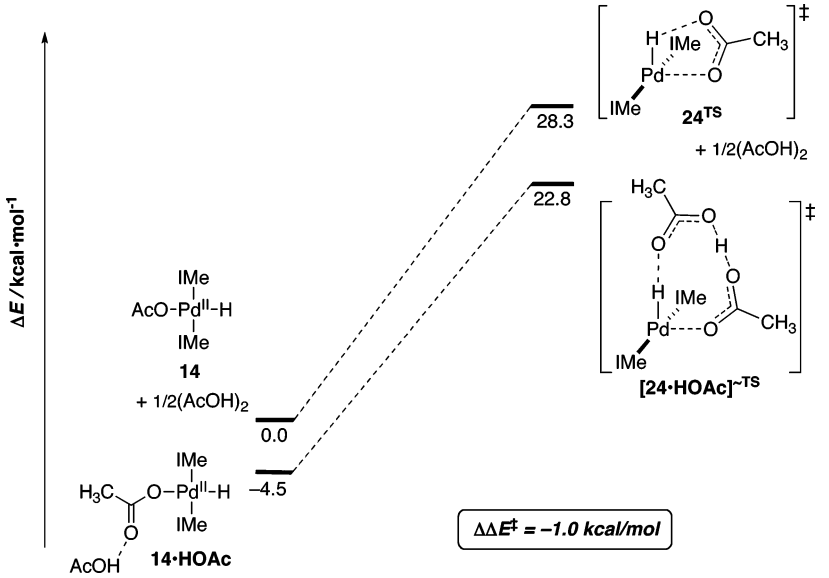

Figure 12. Influence of exogenous AcOH on the energy barrier ($DE^{\ddagger}$) for the reductive elimination of AcOH from complex **14**.

for H atom abstraction from **14·HOAc** than from **14**: $\Delta E^{\ddagger} =$ 16.8 versus 16.0 kcal/mol, respectively ($\Delta\Delta E^{\ddagger} = +0.9$ kcal/mol, Figure 11). Although this energy difference is small, the result is consistent with the trend described previously for H atom abstraction from **14** and the methyl−hydride complex **16**: the more weakly donating acetate ligand trans to the hydride contributes to a higher activation barrier relative to the strongly donating trans methyl group. The hydrogen-bonded acetate ligand in **14·HOAc** is expected to be even less donating than acetate; therefore, the barrier to H atom abstraction from **14·HOAc** relative to **14** should increase.

Exogenous acetic acid has the opposite effect on the HX reductive elimination pathway. Reductive elimination of acetic acid proceeds with a lower barrier from **14·HOAc** than from **14**: $\Delta E^{\ddagger} = 27.3$ vs 28.3 kcal/mol, respectively ($\Delta\Delta E^{\ddagger} = -1.0$ kcal/mol, Figure 12). The approximate transition state **[24·HOAc]**$^{\sim TS}$ (Figure 13),[41] identified for the reductive elimination of AcOH from **14·HOAc**, corresponds to an acetic adduct of **24**^{TS}. The calculations reveal that acetic acid stabilizes the transition state **24**^{TS} to a greater extent than the ground state **14**, an effect that appears to reflect the greater ionic character of the acetate fragment in the **24**^{TS} relative to **14** as described earlier.[42]

Experimental Implications. The DFT calculations indicate that the hydrogen atom abstraction pathway is inhibited and that the HX reductive elimination pathway is promoted by added carboxylic acid. Although the magnitude of the effect is quite small in both cases, the trends observed for the two pathways (i.e., inhibition vs promotion) reflect those expected from the chemical properties of the transition states. The DFT results for the HX reductive elimination pathway are consistent with the experimental rate enhancement observed for palladium−hydride oxygenation in the presence of added carboxylic acid. Therefore, we tentatively propose that the experimental reaction

(40) We restrict our analysis in this section to a comparison of electronic total energies ($\Delta E°$ and $\Delta E^{\ddagger}$) rather than free energies ($\Delta G°$ and $\Delta G^{\ddagger}$) because identification of a true transition state for the HX reductive elimination pathway has thus far been elusive and prevents us from calculating a free energy of activation ($\Delta G^{\ddagger}$) for this mechanism.

(41) The approximate transition-state structure **[24·HOAc]**$^{\sim TS}$ possesses two imaginary frequencies (−132.7 and −16.8 cm^{-1}). Attempts to optimize a true transition state (i.e., a structure with a single imaginary frequency) have been complicated by the fact that the potential energy surface in the region of the saddle point appears to be quite flat.

(42) We note that water (the stoichiometric byproduct of O_2 reduction) and other hydrogen-bond donating molecules present under catalytic reaction conditions (substrates, products, and additives) could mimic the effect of acetic acid.

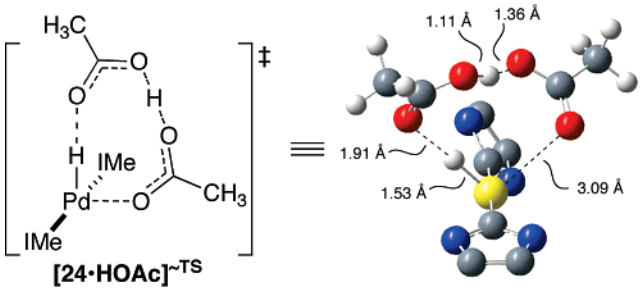

Figure 13. Ball-and-stick representation and key bond lengths for the approximate transition-state structure **[24·HOAc]**$^{\sim TS}$.

of *trans*-$(IMes)_2Pd(H)(O_2CPh)$ (**12**) with molecular oxygen forms the hydroperoxide product *trans*-$(IMes)_2Pd(OOH)(O_2CPh)$ (**13**) by sequential reductive elimination of benzoic acid, oxygenation of $(IMes)_2Pd^0$, and protonolysis of a Pd−O bond by benzoic acid.

The calculations outlined in this study make several other important predictions relevant to ongoing experimental efforts to elucidate the mechanism of the oxygenation of **12**. The hydrogen atom abstraction pathway should exhibit a bimolecular rate law, first order in [Pd−H] and $[O_2]$, and a large isotope effect. Indeed, experimental and theoretical studies of the oxygenation of (PCP)Pd(H) complex **10** support the H atom abstraction pathway for this reaction (eq 1).[8b,9] In contrast, the calculated energy profile for the HX reductive elimination pathway in Figure 8 predicts that palladium−hydride oxygenation by this mechanism will exhibit a unimolecular rate law, first order in [Pd−H] but zero order in $[O_2]$. Furthermore, the nonlinear transition state for the reductive elimination step suggests that a relatively small isotope effect might be observed. These predictions suggest straightforward experiments to distinguish between the two pathways for the oxygenation of **12** derived from our DFT calculations.

Conclusion

The calculations outlined previously have evaluated four possible pathways for the reaction of molecular oxygen with the palladium^{II}−hydride complex *trans*-$(NHC)_2Pd(H)OAc$ to generate the hydroperoxide product *trans*-$(NHC)_2Pd(OOH)OAc$. The η^2-peroxo−Pd^{IV} and the O_2 insertion pathways have been excluded because they proceed through intermediates that are prohibitively high in energy; however, the other two pathways, involving hydrogen atom abstraction and HX reductive elimination, exhibit barriers that are very similar in energy. Calculations probing the role of exogenous carboxylic acid on the reaction support the HX reductive elimination pathway for the oxygenation of *trans*-$(NHC)_2Pd(H)(O_2CR)$ complexes; however, this computational evidence remains somewhat tentative. Nevertheless, the results of this study suggest further experiments that should enable distinction between the mechanistic possibilities.

Another important conclusion from this study is the potential mechanistic ambiguity associated with catalyst reoxidation in Pd-catalyzed aerobic oxidation reactions. Oxygenation of a palladium−hydride intermediate by the HX reductive elimination pathway (Scheme 2, **B** → **C** → **D** → **E**) reflects the traditional Pd^{II}/Pd^0 catalytic cycle (Scheme 1A). The hydrogen atom abstraction mechanism, however, bypasses Pd^0 and results in the direct conversion of a palladium^{II}−hydride into a palladium^{II}−hydroperoxide (Scheme 2, **B** → **E**). The results

Chart 1. Common Catalyst Systems for Palladium-Catalyzed Aerobic Oxidation Reactions

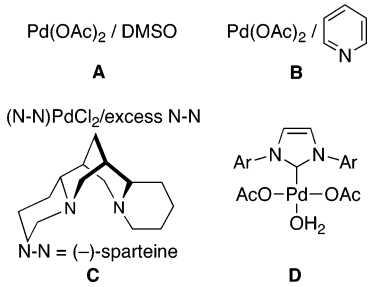

outlined here suggest that the preferred pathway will depend on the reaction conditions and the ancillary ligands coordinated to Pd. Strong donor ligands, particularly those trans to hydride, lower the barrier for the HAA mechanism, as observed in the oxygenation of *trans*-$(NHC)_2Pd(H)(CH_3)$ and the (PCP)Pd(H) complex **10**. The ionic character of the HX reductive elimination step suggests that basic ligands (e.g., carboxylates) susceptible to heterolytic dissociation from the Pd center will favor the HX reductive elimination pathway. The latter conclusion implies that polar solvents that facilitate Pd−X ionization also might favor the HX reductive elimination pathway.

Despite the remaining uncertainties associated with the mechanism of palladium−hydride oxygenation, we speculate that the HX reductive elimination pathway is the most likely mechanism for catalyst oxidation under typical reaction conditions. This hypothesis reflects the results of the present study together with consideration of the most common catalyst systems for Pd-catalyzed aerobic oxidation reactions (Chart 1).[1] None of the catalyst systems except **D** possesses strong donor ligands that would favor H atom abstraction, and the presence of only a single *N*-heterocyclic carbene in **D** suggests that it will be even less likely than **12** to react via the HAA pathway. The presence of acetate ligands in catalyst systems **A**, **B**, and **D** should facilitate HX reductive elimination, particularly if the acetate can occupy a cis coordination site with respect to the hydride. The (−)-sparteine catalyst **C** does not have carboxylate ligands; however, the excess (−)-sparteine employed in these reactions might serve as a Brønsted base to promote HX reductive elimination by a pathway analogous to that in eq 13. The role of (−)-sparteine as a Brønsted base in other steps in Pd-catalyzed oxidation reactions is well-documented.[1c−e] Future studies to test these hypotheses, both computationally and experimentally, are ongoing.

Acknowledgment. We thank Prof. C. R. Landis and M. M. Konnick for valuable discussions. Financial support and computational resources from the following agencies and the UW Parallel Computing Center are gratefully acknowledged: NSF (CHE-0094344 and CHE-0091916), TeraGrid (TG CHE-060010T), and gifts from the Intel Corporation.

Supporting Information Available: NHC model complex energetic comparison, gas-phase and toluene-solvated total energies with thermodynamic corrections, geometry optimization details, frequencies, Cartesian coordinates for optimized complexes, and complete refs 13 and 26. This material is available free of charge via the Internet at http://pubs.acs.org.

JA069037V